AIAA JOURNAL
Vol. 37, No. 8, August 1999

Use of a Direct Boundary Element Method for Pin-Loaded Plates

Chien-Chang Lin,* Chuen-Horng Lin,† and James T. S. Wang‡
National Chung-Hsing University, Taichung 402, Taiwan, Republic of China

A previously developed direct boundary element method for analyzing stresses around pin-loaded holes of composite laminates has been extended with a refined and improved computational algorithm. The method, procedure, and computer program are verified by elasticity solutions in polar coordinates for eyebars and plates having an open, as well as loaded, hole. In turn, boundary tractions generated by the direct boundary element method allowing direct application of elasticity solutions are presented. Such a scheme, which couples the boundary element and analytical methods, appears to be plausible, accurate, and efficient for practical applications.

Nomenclature

a	= pin radius
b	= outer radius of an annulus
c_{ij}	= stiffness constants
D	= hole diameter
E	= Young's modulus of isotropic material
E_{11}	= Young's modulus in direction 1
E_{22}	= Young's modulus in direction 2
e	= clearance between the hole and the pin
F_{ij}	= fundamental solution for traction
G	= shear modulus of isotropic material
G_{12}	= shear modulus in 1–2 plane
H_{ij}	= fundamental solution for displacement
h	= thickness of the plate
L	= length of the plate
p_i, p_o	= internal and external pressures
R	= hole radius
t_x, t_y	= traction components of the hole edge
u_r, u_ϕ	= radial displacement and circumferential displacement
u_x, u_y	= displacement components of the hole edge
W	= width of the plate
α	= one-half of the total angle of contact
β	= one-half of the total contact angle of no-slip regions
δ	= pin displacement
μ	= coefficient of static friction
ν	= Poisson's ratio of isotropic material
ν_{12}	= Poisson's ratio in 1–2 plane
σ_r, σ_ϕ, $\sigma_{r\phi}$	= stress components
ϕ	= polar angle with respect to the hole center
ψ	= polar angle with respect to the pin center

I. Introduction

PIN-LOADED plates of isotropic and composite materials have been investigated by many authors. Analytical methods[1–5] were generally used in earlier studies on stress analysis of the problem. In the investigations concerning strength and failure of a pin-loaded plate[6–10] and analyses involving multiple holes,[11,12] finite element methods were used. Waszczak and Cruse[13] modeled pin-loaded plates by a finite element method to assess various failure limits using experimental data provided by General Dynamics Corporation. Boundary element methods[14,15] have also been developed and used for pin-loaded composite plates. In all of these studies, the contact stress between the pin and the hole is assumed to vary as a cosine function of the polar angle for smooth pins. Whereas such a preassumed variation of the contact stress around the hole edge deviates from the true distribution, it greatly simplifies the analysis. There are studies accounting for the interaction between the pin and the hole. Hyer and Klang[16] and Hyer et al.[17] used a complex Fourier series in conjunction with boundary collocations. Yogeswaren and Reddy[18] and Rahman and Rowlands[19] used a Lagrange multiplier method. Finite element methods,[20–22] as well as a boundary element method,[23] have also been used. Some experimental studies can be found in Refs. 24–27.

A direct boundary element method was established and used successfully by Lin and Lin[23] in the study of stresses around pin-loaded holes of composite laminates. Although the numerical results presented by Lin and Lin[23] are physically consistent and reasonable and agree well with other existing solutions by Hyer and Klang,[16] the method and level of accuracy have not been verified in any way. Also, the procedure and computational algorithm established earlier by Lin and Lin[23] only allow the determination of stresses around the edge of the pin-loaded hole. In this study, the method has been extended to include the determination of stresses as well as displacements at any point in the plate, and the computer program has been modified somewhat for improving the computational efficiency. Whereas the refined direct boundary element method has shown its effectiveness for determining stresses and deformation of pin-loaded laminates, it is necessary and desirable to somehow assess the level of accuracy and provide added confidence in the method. A number of simple cases with readily known elasticity solutions are considered for verification purposes. In turn, when tractions and/or displacements along two concentric circles determined from the boundary element method (as shown in Fig. 1) are properly represented by continuous functions, stresses and displacements can be routinely and accurately determined from the elasticity solutions in the regions bounded by these two concentric circles. Although the displacements and stresses in the pin-loaded plate can be calculated by the boundary element method once the boundary tractions and/or displacements are determined, it often requires some judgement and experience in using the boundary element program and numerical integrations involved in the process. This is particularly true for computing displacements and stresses at interior points close to or on the boundary. Hence, it appears to be easier and more direct by specifying the tractions and/or displacements along two concentric circles on the basis of the boundary element solutions and subsequently using the elasticity solutions for points between these circular boundaries. Such a scheme, coupling the boundary element and exact elasticity solutions, would provide a simple, direct, and accurate determination of deformation and stress distribution within these circular boundary lines. This is a desirable procedure for practical applications inasmuch as the failure of pin-loaded plates generally occurs at and near the loaded hole edge. Accordingly, we have considered realistic pin-loaded structural components for verifying the direct boundary element method. In addition, they are used to demonstrate the procedure of using the coupled boundary

Received 7 July 1998; revision received 5 January 1999; accepted for publication 6 January 1999.

*Professor, Department of Applied Mathematics; cclin@amath.nchu.edu.tw. Associate Fellow AIAA.

†Graduate Assistant, Department of Applied Mathematics; currently Associate Professor, National Taichung Institute of Commerce, Taichung 404, Taiwan, Republic of China.

‡Visiting Research Chair Professor, Department of Applied Mathematics; on leave from Georgia Institute of Technology, Atlanta, GA 30332.

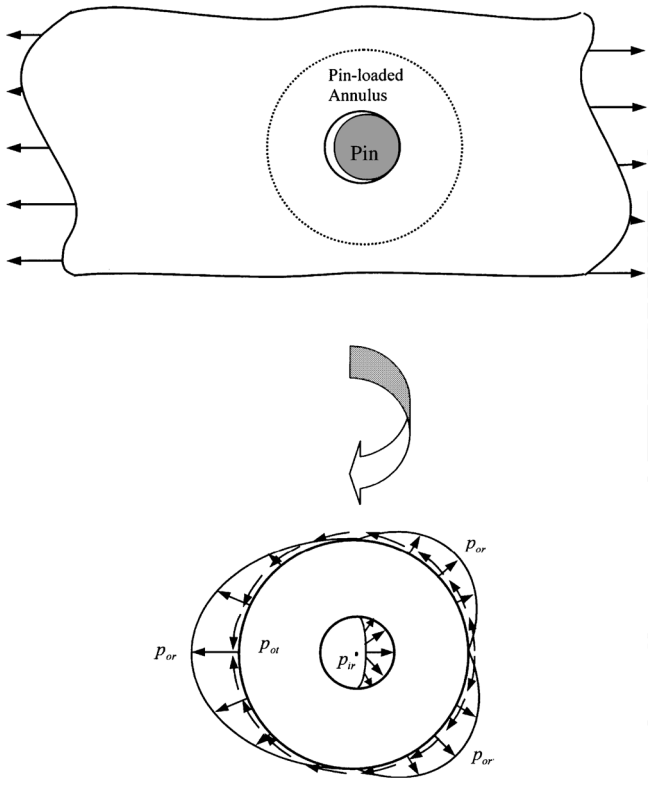

Fig. 1 Boundary tractions for pin-loaded annulus.

element and elasticity solutions for points within two concentric circular boundaries including the hole edge. For the convenience, we refer to this region as the pin-loaded annulus.

II. Direct Boundary Element Method for Pin-Loaded Plates

Inasmuch as the purpose of the study is to verify the direct boundary element method established for the investigation of pin-loaded plates, only one-half of a structure is modeled because of symmetry. Generally orthotropic laminates loaded by a rigid pin are considered in the general formulation.

A. Basic Relations and Conditions of Contact

Orthotropic laminates of finite size subjected to a pin displacement δ or load P in the longitudinal x direction are considered. Effects of clearance and friction between a rigid pin and the hole edge are accounted for in the general formulation. The geometry, coordinate systems, and some symbols are shown in Fig. 2. The angle 2α represents the total contact region, whereas the angle 2β identifies the no-slip region.

The relations of the compatibility in displacement must be satisfied on the no-slip contact surface $(-\beta < \phi < \beta)$ at $r = R$ as follows:

$$R\cos\phi + u_x = a\cos\psi + (e+\delta) \qquad (-\beta < \phi < \beta) \quad (1a)$$

$$R\sin\phi + u_y = a\sin\psi \qquad (-\beta < \phi < \beta) \quad (1b)$$

where ϕ and ψ are polar angles of coordinates fixed on the plate and pin, respectively; u_x and u_y are displacements of the hole edge in the x and y directions, respectively; e is the clearance between the hole and the pin; and δ is the longitudinal movement of the pin beyond the first contact. In the slip region $(\beta \le \phi < \alpha)$ and $(-\alpha < \phi \le -\beta)$ at $r = R$, the following compatibility of the displacement in the radial direction of the pin and hole edge:

$$u_r = u_x\cos\phi + u_y\sin\phi$$

$$= [e+\delta+a\cos\psi]\cos\phi + a\sin\psi\sin\phi - R$$

$$(-\alpha < \phi \le -\beta \quad \text{and} \quad \beta \le \phi < \alpha) \quad (2a)$$

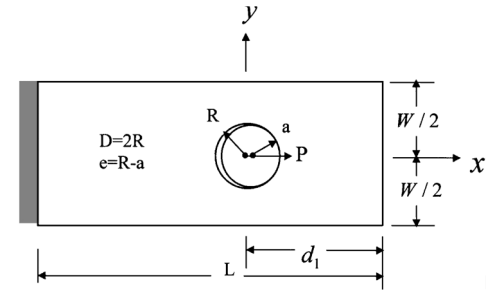

a) Dimensions of pin-loaded laminate

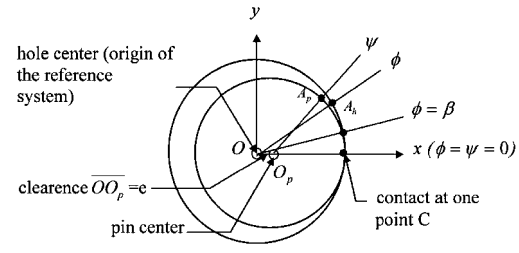

b) Configuration of pin-loaded hole before deformation

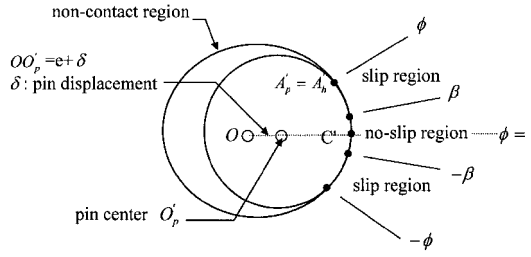

c) Configuration of pin-loaded hole after deformation

Fig. 2 Geometry and coordinate systems for pin-loaded laminates.

and the force condition

$$|\tau_{r\phi}| = \mu|\sigma_r| \qquad (-\alpha < \phi \le -\beta \quad \text{and} \quad \beta \le \phi < \alpha) \quad (2b)$$

must be satisfied, where u_r is the radial displacement of the hole edge and μ is the coefficient of static friction between the pin and hole edge. In the noncontact region along the hole edge $(\alpha \le \phi \le 2\pi - \alpha)$, the radial and shear stresses σ_r and $\tau_{r\phi}$ are zero.

Equations (1a), (1b), and (2a) involve the angle ψ and ϕ, which identify the matching points of the pin surface and the hole edge after deformation. Hyer and Klang[16] and Hyer et al.[17] simply take $\psi = \phi$ without giving specific explanation, whereas Lin and Lin[23] used $a\psi = R\phi$ with reasons made on the basis of kinematics.

B. Direct Boundary Element Method

A direct boundary element method was developed and used by Lin and Lin[23] for determining stresses around pin-loaded holes of composite laminates. The basic equation for determining boundary displacement with no body force is

$$\kappa u_i(\xi) = \int_s [H_{ij}(x,\xi)t_j(x) - F_{ij}(x,\xi)u_j(x)]\,\mathrm{d}s(x) \qquad (3)$$

in which κ equals 1 when point ξ is inside of S, $\frac{1}{2}$ when ξ lies on the smooth boundary surface S, and 0 when ξ is outside of S; F_{ij} and H_{ij} are fundamental solutions for traction and displacements, respectively, at a point x in i direction due to a unit force applied at point ξ in the j direction; and u_j and t_j are the displacement and traction, respectively. Other details and discussions on the use of integral formulations for the direct boundary element method and the fundamental solution can be found in Ref. 23. The discretization of the boundary of the pin-loaded plate used by Lin and Lin[23] has been refined and improved for enhancing computational efficiency. Although details can be found in Ref. 28, a brief account is presented here.

The entire boundary is divided into M quadratic elements, which consist of M_{c1}, M_{c2}, and M_{nc} elements for slip contact regions, no-slip contact regions, and the remaining non-contact hole edge and the exterior boundary of the plate, respectively. Each element has three nodes with two end nodes jointed to adjacent elements. Each node of an element has two displacements and two traction components. Because of geometric compatibility, only two displacement components for each set of the common end nodes joined to adjacent elements are used, although two traction components are required to describe the force state at each end node. From Eq. (3), we can relate the displacement vector of a nodal point p in terms of tractions or displacements at all $(2M)$ nodal points on the entire boundary as

$$\frac{1}{2}\{u_i^p\} = \sum_{q=1}^{M}\left[\int_{S_q} H_{ij}^{pq} N^K \, dS\right]\{t_j^K\}^q - \sum_{q=1}^{M}\left[\int_{S_q} F_{ij}^{pq} N^K \, dS\right]\{u_j^K\}^q$$
$$(\bar{p} = 1, 2, \ldots, 2M, \qquad K = 1, 2, 3, \qquad i, j = 1, 2) \quad (4)$$

where N^K is the shape function for the Kth node in the qth element. In the slip region along the contact surface of the hole boundary, one requires one displacement component due to the geometric compatibility Eq. (2a) and one traction component for the force condition Eq. (2b) to be specified at each of the $2M_{c1}$ nodal points. Thus, we can rewrite Eq. (4) in the form

$$[\bar{F}]\{u\} + [\bar{F}_B] = [\bar{H}]\{t\} \quad (5)$$

where

$$\left[\bar{F}_{i,j-1}^{M_{c1}}\right] = \left[F_{i,j-1}^{M_{c1}}\right] - \left[F_{i,j}^{M_{c1}}\right]\cot\phi$$
$$\left[\bar{F}_{B_i}^{M_{c1}}\right] = \left[F_{B_i}^{M_{c1}}\right] + \left\{\left[\delta + e + a\cos\left(\frac{R}{a}\phi\right)\right]\cos\phi + a\sin\left(\frac{R}{a}\phi\right)\sin\phi - R\right\}\frac{\left[F_{i,j}^{M_{c1}}\right]}{\sin\phi}$$
$$\left[\bar{F}_{i,j}^{M_{c1}}\right] = 0$$
$$i = 1, 2, \ldots, 4M, \qquad j = 2, 4, \ldots, 4M_{c1} \quad (j = \text{even}) \quad (6)$$

and

$$\left[\bar{H}_{i,j-1}^{M_{c1}}\right] = \left[H_{i,j-1}^{M_{c1}}\right] + \left[H_{i,j}^{M_{c1}}\right]\left(\frac{\sin\phi + \mu\cos\phi}{\cos\phi - \mu\sin\phi}\right)$$
$$\left[\bar{H}_{i,j}^{M_{c1}}\right] = 0$$
$$i = 1, 2, \ldots, 4M, \qquad j = 2, 4, \ldots, 6M_{c1} \quad (j = \text{even}) \quad (7)$$

in which $[\bar{F}]$, $[\bar{H}]$, and $[\bar{F}_B]$ are $4M \times (4M_{nc} + 2M_{c1} + 4M_{c2})$, $4M \times (6M_{nc} + 2M_{c1} + 4M_{c2})$, and $4M \times 1$ matrices, respectively; $\{u\}$ and $\{t\}$ have the dimensions of $(4M_{nc} + 2M_{c1} + 4M_{c2}) \times 1$ and $(6M_{nc} + 2M_{c1} + 4M_{c2}) \times 1$, respectively. Using the $6M_{nc} + 4M_{c2}$ tractions or displacements given from the boundary conditions at all $2M_{nc}$ and $2M_{c2}$ nodal points, Eq. (5) can be rewritten in the following form:

$$[A]\{X\} = [B]\{Y\} \quad (8)$$

where $[A]$ is a $4M \times 4M$ matrix and $\{X\}$ contains the $4M \times 1$ unknown traction and displacement components, $[B]$ is a $4M \times (6M_{nc} + 4M_{c2})$ matrix, and $\{Y\}$ contains the given $(6M_{nc} + 4M_{c2})$ boundary quantities. Note that if M_c number of corner points on the nc part of boundary can be identified, then $6M_{nc}$ can be reduced to $(4M_{nc} + 2M_c)$. Clearly, if the entire boundary is perfectly smooth, $6M_{nc}$ can further be reduced to $4M_{nc}$.

The authors' earlier work, presented in Ref. 23, only allows the determination of stresses around the edge of the pin-loaded hole. The method has been extended to include the determination of stresses as well as displacements at any point in the plate to allow eventual design applications. Using the fundamental solution in conjunction with the displacements and tractions of the boundary elements, the displacement at any point $\bar{p}$ of the structure can be determined from the following equation:

$$\left[u_i^{\bar{p}}\right] = \sum_{q=1}^{M}\left[\int_S H_{ij}^{\bar{p}q} N^K \, dS\right]\{t_j^K\}^q - \sum_{q=1}^{M}\left[\int_S F_{ij}^{\bar{p}q} N^K \, dS\right]\{u_j^K\}^q$$
$$(i, j = 1, 2) \quad (9)$$

and the strain components $\varepsilon_x(\varepsilon_{11})$, $\varepsilon_y(\varepsilon_{22})$, and $\gamma_{xy}(2\varepsilon_{12})$ can be determined subsequently. Through Hooke's law, we obtain the stress components as follows:

$$\left[\sigma_{ik}^{\bar{p}}\right] = \sum_{q=1}^{M}\left[\int_S D_{ijk}^{\bar{p}q} N^K \, dS\right]\{t_j^K\}^q - \sum_{q=1}^{M}\left[\int_S U_{ijk}^{\bar{p}q} N^K \, dS\right]\{u_j^K\}^q$$
$$(k = 1, 2) \quad (10)$$

in which D_{ijk} and U_{ijk} contain the material constants and derivatives of H_{ij} and F_{ij} with respect to ξ_k. Although Eqs. (9) and (10) are presented explicitly, the integrals involved in the equations must be determined numerically. This may cause some difficulty in the computational process.

III. Elasticity Solutions for Annulus Plates

For the eventual verification purpose and applications of a scheme that couples boundary element and elasticity solutions, we briefly present basic results for stresses and displacements for annulus plates from the elasticity solutions.

The general solution of the Airy stress function Φ satisfying the biharmonic equation for isotropic materials is available in textbooks on elasticity such as by Timoshenko and Goodier.[29] Because the general solution of Φ will eventually be used for pin-loaded plates considered in the study, the part of the solution that is symmetrical with respect to the x axis is given here:

$$\Phi = a_0 \ell n\, r + b_0 r^2 + \frac{a_1}{2} r\phi\sin\phi + \left(b_1 r^3 + a_1' r^{-1} + b_1' r \ell n\, r\right)\cos\phi + \sum_{n=2}^{\infty}\left(a_n r^n + b_n r^{n+2} + a_n' r^{-n} + b_n' r^{-n+2}\right)\cos n\phi \quad (11)$$

in which a_n, b_n, a_n', and b_n' for $n = 0$–∞ are constants of integration. The relations between stresses and stress function Φ in polar coordinates without body force are

$$\sigma_r = \frac{1}{r}\frac{\partial\Phi}{\partial r} + \frac{1}{r^2}\frac{\partial^2\Phi}{\partial\phi^2}, \qquad \sigma_\phi = \frac{\partial^2\Phi}{\partial r^2}$$
$$\tau_{r\phi} = \frac{1}{r^2}\frac{\partial\Phi}{\partial\phi} - \frac{1}{r}\frac{\partial^2\Phi}{\partial\phi^2} = -\frac{\partial}{\partial r}\left(\frac{1}{r}\frac{\partial\Phi}{\partial\phi}\right) \quad (12)$$

Although solutions for stresses may be determined by direct differentiation of Φ in Eq. (11) using Eqs. (12), the explicit expressions are not commonly available in textbooks. We have derived them and present them for the convenience of readers:

$$\sigma_r = a_0 r^{-2} + 2b_0 + \left(a_1 r^{-1} + 2b_1 r - 2a_1' r^{-3} + b_1' r^{-1}\right)\cos\phi + \sum_{n=2}^{\infty}\left[n(1-n)a_n r^{n-2} + (n+2-n^2)b_n r^n - n(1+n)a_n' r^{-(n+2)} + (-n+2-n^2)b_n' r^{-n}\right]\cos n\phi \quad (13)$$

$$\sigma_\phi = -a_0 r^{-2} + 2b_0 + \left(6b_1 r + 2a_1' r^{-3} + b_1' r^{-1}\right)\cos\phi + \sum_{n=2}^{\infty}\left[n(n-1)a_n r^{n-2} + (n+2)(n+1)b_n r^n + n(n+1)a_n' r^{-(n+2)} + (-n+2)(-n+1)b_n' r^{-n}\right]\cos n\phi \quad (14)$$

$$\tau_{r\phi} = \left(2b_1 r - 2a_1' r^{-3} + b_1' r^{-1}\right)\sin\phi + \sum_{n=2}^{\infty}\left[n(n-1)a_n r^{n-2} + n(n+1)b_n r^{n} - n(n+1)a_n' r^{-(n+2)} + n(1-n)b_n' r^{-n}\right]\sin n\phi \tag{15}$$

Displacements are determined by using the following stress–strain-displacement relations in conjunction with Eqs. (13–15):

$$\varepsilon_r = \frac{\partial u_r}{\partial r} = \frac{1}{E}(\sigma_r - \nu\sigma_\phi), \qquad \varepsilon_\phi = \frac{u_r}{r} + \frac{1}{r}\frac{\partial u_\phi}{\partial \phi} = \frac{1}{E}(\sigma_\phi - \nu\sigma_r)$$
$$\gamma_{r\phi} = \frac{1}{r}\frac{\partial u_r}{\partial \phi} + \frac{\partial u_\phi}{\partial r} - \frac{u_\phi}{r} = \frac{1}{G}\tau_{r\phi} \tag{16}$$

The general solutions for the radial displacement u_r and circumferential displacement u_ϕ are obtained as follows:

$$u_r = \frac{1}{E}\Bigg\{-(1+\nu)a_0 r^{-1} + 2b_0(1-\nu)r + \left[a_1 \ell_n r + b_1(1-3\nu)r^2 + a_1'(1+\nu)r^{-2} + b_1'(1-\nu)\ell_n r\right]\cos\phi - \sum_{n=2}^{\infty}\left[n(1+\nu)a_n r^{n-1} + [n(1+\nu) - 2(1-\nu)]b_n r^{n+1} - n(1+\nu)a_n' r^{-(n+1)} - [n(1+\nu) + 2(1-\nu)]b_n' r^{-(n-1)}\right]\cos n\phi\Bigg\} + f(\phi) \tag{17}$$

$$u_\phi = \frac{1}{E}\Bigg\{\left[-(\nu + \ell_n r)a_1 + (5+\nu)b_1 r^2 + (1+\nu)a_1' r^{-2} + (1-\nu)b_1'(1-\ell_n r)\right]\sin\phi + \sum_{n=2}^{\infty}\left[n(1+\nu)a_n r^{n-1} + [n(1+\nu)+4]b_n r^{n+1} + n(1+\nu)a_n' r^{-(n+1)} + [n(1+\nu) - 4]b_n' r^{-(n-1)}\right]\sin n\phi\Bigg\} - \int f(\phi)\,d\phi + g(r) \tag{18}$$

The arbitrary functions $f(\phi)$ and $g(r)$ in Eqs. (17) and (18) for deformation symmetrical with respect to the x axis are

$$f(\phi) = J\cos\phi, \qquad g(r) = 0 \tag{19}$$

in which J is an integration constant representing a rigid-body displacement in the x direction.

IV. Verification of the Direct Boundary Element Method

To verify the direct boundary element method numerically, the following three classes of problems are considered: 1) isotropic annulus plates under uniform internal and external pressures, 2) rectangular orthotropic plates with an open hole under uniform tension, and 3) pin-loaded isotropic eyebar plates. Note that the computer program developed is applicable to isotropic as well as orthotropic plates.

A. Isotropic Annulus Plates

The elasticity solutions for isotropic annulus plates under uniform pressures may be found in textbooks in elasticity such as Timoshenko and Goodier.[29] The stress components and radial displacement u_r are as follows:

$$\sigma_r = \frac{R^2 b^2 (p_o - p_i)}{b^2 - R^2}\frac{1}{r^2} + \frac{p_i R^2 - p_o b^2}{b^2 - R^2} \tag{20}$$

$$\sigma_\phi = -\frac{R^2 b^2 (p_o - p_i)}{b^2 - R^2}\frac{1}{r^2} + \frac{p_i R^2 - p_o b^2}{b^2 - R^2} \tag{21}$$

$$u_r = \frac{1}{E}\left[-\frac{R^2 b^2 (p_o - p_i)}{b^2 - R^2}\frac{(1+\nu)}{r} + \frac{p_i R^2 - p_o b^2}{b^2 - R^2}(1-\nu)r\right] \tag{22}$$

where R and b are the inner and outer radii of the cylinder and p_i and p_o are internal and external pressures, respectively.

An annulus plate with $E = 57.85$ GPa and $\nu = 0.31$ under various loading conditions of $p_i = p_o$, $p_i = 4p_o$, and $p_i = p_o/4$ are considered. The plate has an outer radius $b/R = 4$. A total of 40 boundary elements are used. The stress distribution and displacement are shown in Figs. 3–5. The results from the direct boundary element method are essentially identical to the exact elasticity solutions given in Eqs. (20–22).

B. Orthotropic Plates with an Open Circular Hole

For the case of an infinite orthotropic plate with a circular hole subjected to a uniform far-field tension, σ in the x direction is considered. The stress distribution in the neighborhood of the hole, according to Lekhnitskii et al.,[30] is as follows:

$$\sigma_\phi = \sigma(E_\phi/E_{xx})[-k\cos^2\phi + (1+n)\sin^2\phi] \tag{23}$$

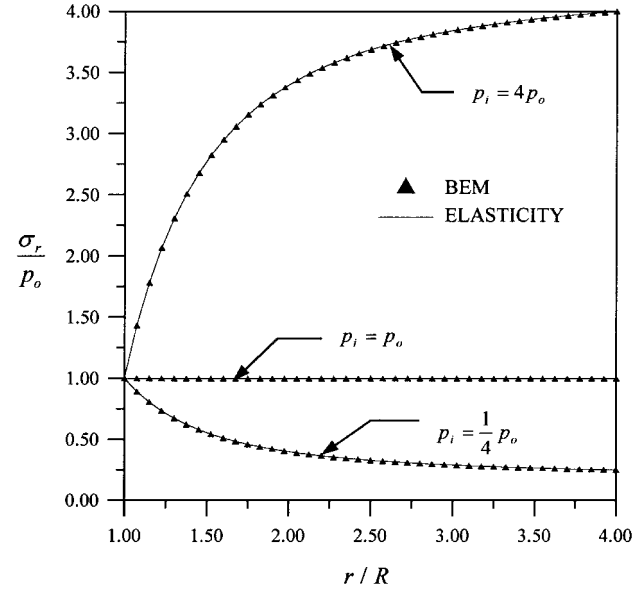

Fig. 3 Radial stress in isotropic annulus plates ($b = 4R$) under uniform pressures.

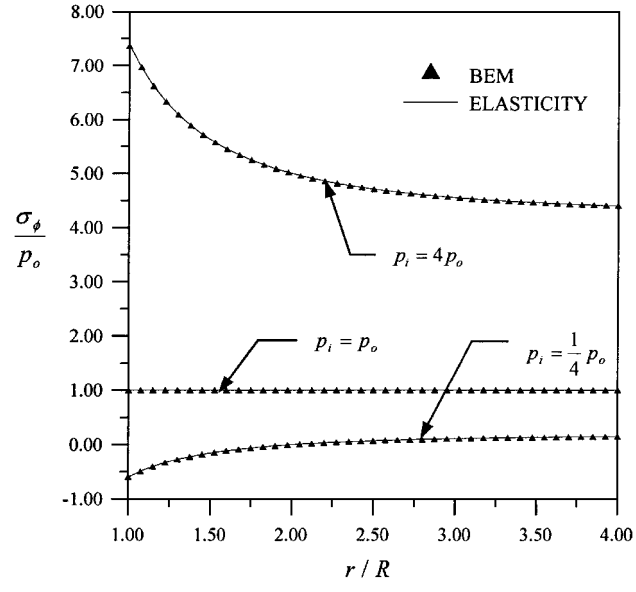

Fig. 4 Circumferential stress in isotropic annulus plates ($b = 4R$) under uniform pressures.

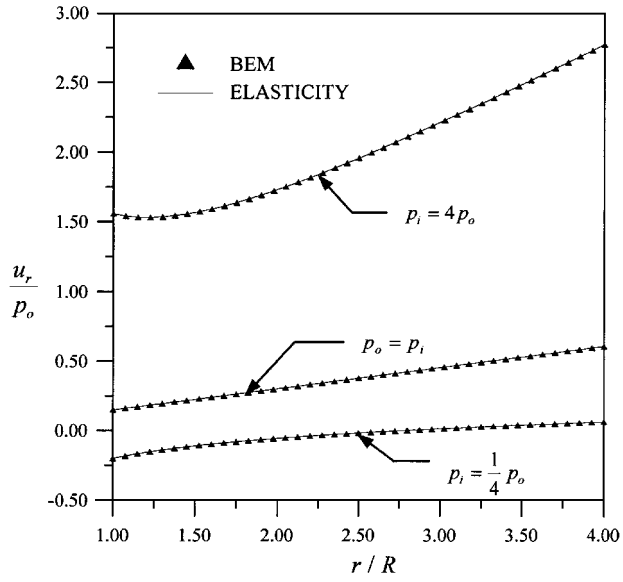

Fig. 5 Displacement of isotropic annulus plates ($b = 4R$) under uniform pressures.

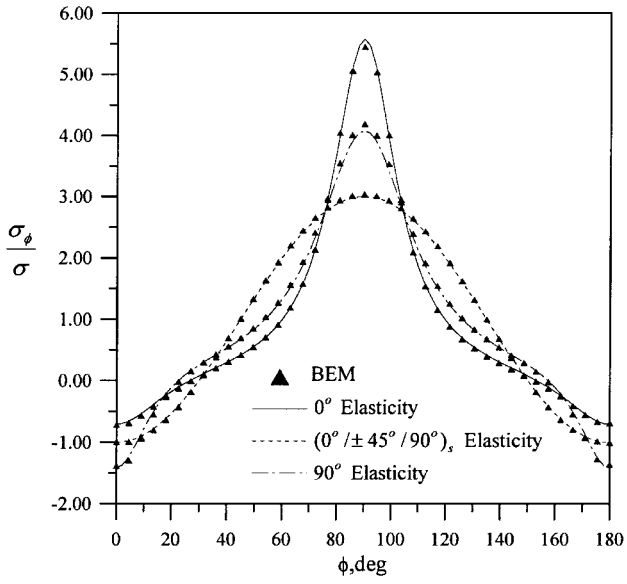

Fig. 6 Circumferential stress along $r = R$ in the plate with an open hole for composite laminates.

where

$$k = \sqrt{E_{xx}/E_{yy}}, \qquad n = \sqrt{2[(E_{xx}/E_{yy}) - \nu_{xy}] + (E_{xx}/G_{xy})} \tag{24}$$

$$\frac{1}{E_\phi} = \frac{\sin^4\phi}{E_{xx}} + \left(\frac{1}{G_{xy}} - \frac{2\nu_{xy}}{E_{xx}}\right)\sin^2\phi\cos^2\phi + \frac{\cos^4\phi}{E_{yy}} \tag{25}$$

where E_{xx}, E_{yy}, G_{xy}, and ν_{xy} are material constants with reference to the x and y coordinates.

An infinite plate for three different composite laminates having 0-, $(0/\pm 45/90)_s$-, and 90-deg stacking sequences are considered for verification. The properties of each layer with respect to the principal material axes are $E_{11} = 1200$ GPa, $E_{22} = 600$ GPa, $G_{12} = 70$ GPa, and $\nu_{12} = 0.6568$. For the boundary element model, we consider $L = W$ and $R = 0.1W = 12.7$ mm, which represents a large plate inasmuch as the edge dimensions are much larger than the hole radius. A total of 49 boundary elements is used. The stress distribution of σ_ϕ per unit applied far-field stress along the hole edge is determined. Comparisons of results are shown in Fig. 6 for 0-, $(0/\pm 45/90)_s$-, and 90-deg laminates, respectively. Present results agree extremely well with the theoretical solutions given in Eq. (23) by Lekhnitskii et al.[30]

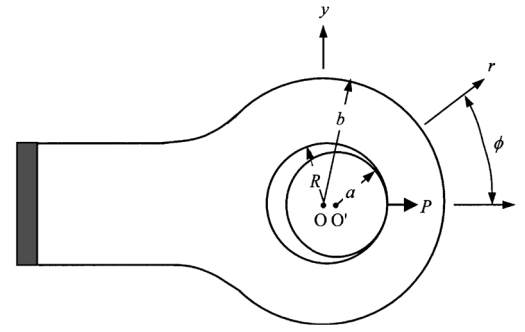

a) Pin-loaded model

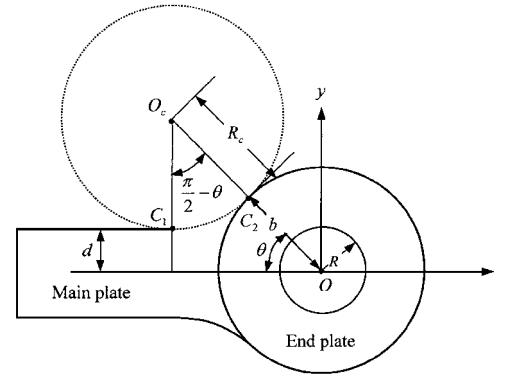

b) Geometry

Fig. 7 Pin-loaded model and geometry of eyebars.

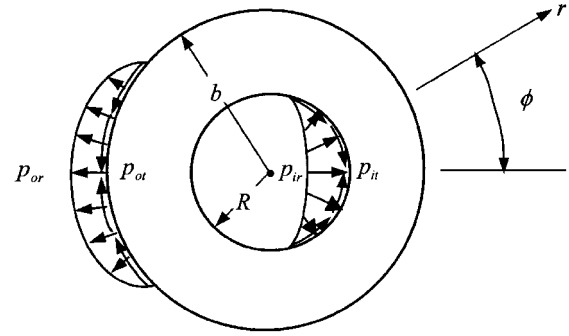

Fig. 8 Boundary tractions of the endplate of eyebars.

C. Pin-Loaded Isotropic Eyebar Plates

Eyebars are commonly used structural components. The geometry, coordinate systems, and some symbols are shown in Fig. 7. The plane geometry of an eyebar of uniform thickness may be viewed as having a rectangular main plate of width $2d$ and a circular end plate of radius b. The endplate is considered as the pin-loaded annulus. The transition from the edge of the main plate to the edge of the endplate is connected by a circular arc of radius R_c with a common tangent at the endpoints C_1 and C_2 of the transition curve. The coordinates of the center of curvature O_c of the transition arc, as shown in Fig. 7b, are

$$x = -(R_c + b)\cos\theta, \qquad y = R_c + d \tag{26}$$

from which

$$\sin\theta = \frac{R_c + d}{R_c + b} \quad \text{or} \quad R_c = \frac{b\sin\theta - d}{1 - \sin\theta} \tag{27}$$

in which θ is the angle locating the endpoints of the transition arc for a given R_c.

Following our consideration mentioned in the Introduction, we first determine the nodal tractions along $r = R$ and b as shown in Fig. 8 by the direct boundary element method. The tractions along the boundaries are then closely represented by convenient continuous functions so that elasticity solutions for the region $R \le r \le b$

and $0 \le \phi \le \pi$ can be obtained for verifying boundary element results. The elasticity solutions then can be used to calculate stresses and displacements directly in this region of pin-loaded annulus for eventual applications. This procedure appears to be simple to use, which would be convenient to practice engineers for checking potential weak points against failure. Accordingly, we represent the variation of each boundary traction component by a linear combination of functions. In this study, sinusoidal functions are used in all illustrative examples as follows:

$$p_{ir} = A_0 + \sum_{m=1}^{m_1} A_m \cos m\phi \qquad \text{for} \qquad 0 \le \phi \le \alpha \tag{28}$$

$$p_{it} = \sum_{m=1}^{m_2} A_m^* \sin m\phi \qquad \text{for} \qquad 0 \le \phi \le \alpha \tag{29}$$

$$p_{or} = B_0 + \sum_{m=1}^{m_3} B_m \cos m\phi \qquad \text{for} \qquad \pi - \theta \le \phi \le \pi \tag{30}$$

$$p_{ot} = \sum_{m=1}^{m_4} B_m^* \sin m\phi \qquad \text{for} \qquad \pi - \theta \le \phi \le \pi \tag{31}$$

in which sufficiently large values of m_1, m_2, m_3, and m_4 are selected to give close representations of the boundary element data. The radial stresses p_{ir} and tangential stresses p_{it} at the nodal points along $r = R$ are calculated from Eq. (8), and p_{or} and p_{ot} at the nodal points on the circle $r = b$ are obtained by Eq. (10). With these given stresses at nodal points and the use of a least-square curve-fitting technique, the values of coefficients A_m, A_m^*, B_m, and B_m^* for describing the boundary traction variations in Eqs. (28–31) are then determined. Hence, Eqs. (28–31) become the analytical boundary conditions for the elasticity problem. Consequently, by using Eqs. (13) and (15), the unknown Fourier coefficients a_n and b_n involved in Eq. (11) can be solved when these boundary conditions are satisfied. The derivation of the general solutions for a_n and b_n in terms of A_m, A_m^*, B_m, and B_m^* can be found Ref. 28. Their results are given in Eqs. (A1–A14) in the Appendix.

For illustrative purposes, we consider an isotropic eyebar, as shown in Fig. 7, with $E = 57.85$ GPa, $\nu = 0.31$, and $e = \mu = 0$ under a uniform far-field stress σ. The geometrical dimensions are $L/R = 16$, $d/R = 2$, $b/R = 4$, $R = 12.7$ mm, $\theta = 45$ deg, and $R_c = 35.921$ mm. A total of 50 boundary elements for the model are used. Because $\mu = 0$ is considered in the present study, $p_{it} = A_m^* = 0$. The boundary tractions of the endplate are shown in Fig. 8. By taking $m_1 = 8$ for p_{ir} and $m_3 = m_4 = 6$ for p_{or} and p_{ot}, the boundary element results are very closely represented by Eqs. (28–31), as shown in Figs. 9 and 10. The contact angle α rounded to the nearest degree is 90 deg. The values of the coefficients for describing boundary traction distributions for this case are given in Table 1. Note that according to the numerical calculations the contact angle for no clearance case ($e = 0$) is essentially independent of σ, and $\sigma = 1$ GPa is used in the numerical examples.

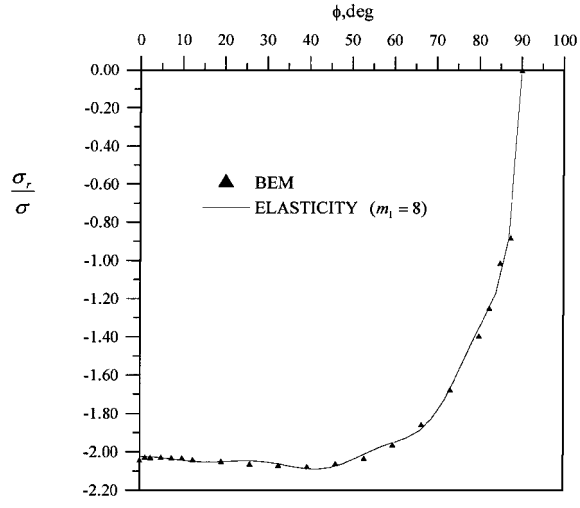

Fig. 9 Normal stress over the contact surface of eyebars: $\alpha = 90$ deg.

Table 1 Constants A_m, B_m, and B_m^* for eyebar: $m_1 = 8, m_3 = m_4 = 6$

m	$q_{ir}(A_m)$	$q_{or}(B_m)$	$q_{ot}(B_m^*)$
0	4,866.706	−106,947.537	——
1	−8,964.784	−185,257.177	−707.412
2	6,975.957	−119,433.405	−1,105.986
3	−4,547.015	−55,857.743	−1,016.611
4	2,439.886	−17,965.561	−594.923
5	−1,045.625	−3,559.933	−204.492
6	339.253	−327.522	−31.517
7	−74.998	——	——
8	8.597	——	——

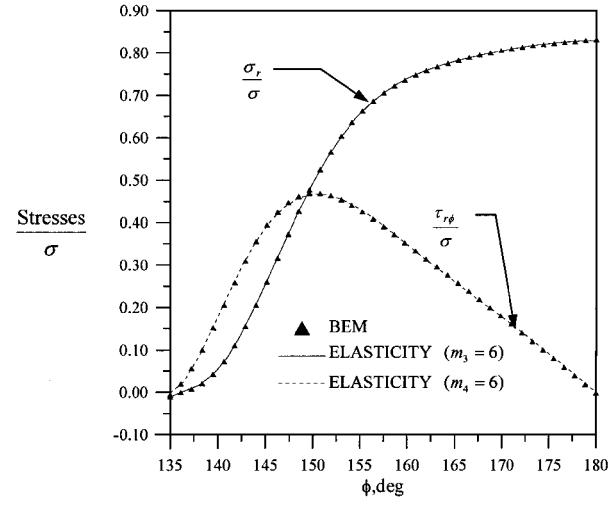

Fig. 10 Stress distribution along the outer surface of the end eyebar plate: $\theta = 45$ deg.

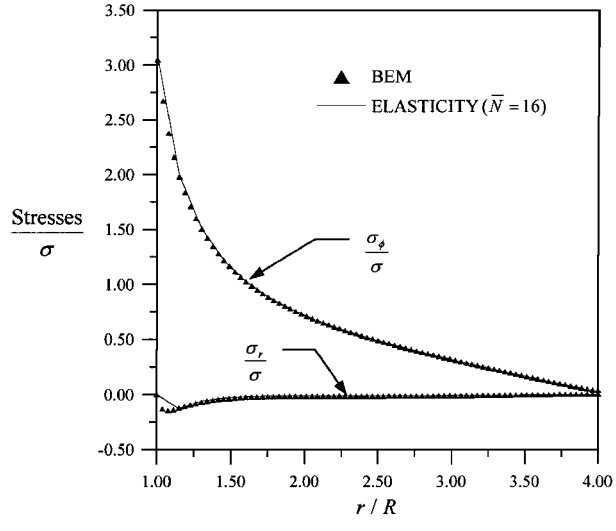

Fig. 11 Stress distribution along $\phi = 90$ deg in the end eyebar plate.

Numerical results obtained by using the explicit expressions have been verified by MATHEMATICA results for confirming the derivations and computer program. The maximum number $\bar{N} = 16$ is found to given sufficiently accurate results and is used throughout. The stress distribution and displacements along $\phi = 90$ deg in the pin-loaded annulus of the eyebar are shown in Figs. 11 and 12. In Fig. 13 the normal stresses σ_r and σ_ϕ and the shear stress $\tau_{r\phi}$ along $r = 2R$ are presented. The results shown that boundary element results and elasticity solutions agree extremely well.

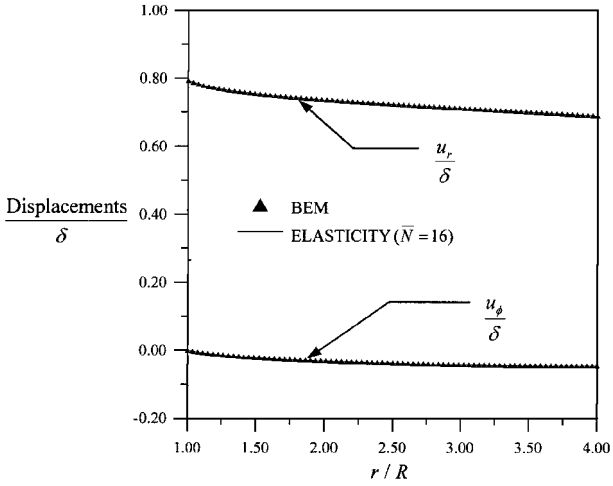

Fig. 12 Displacements along $\phi = 90$ deg in the end eyebar plate.

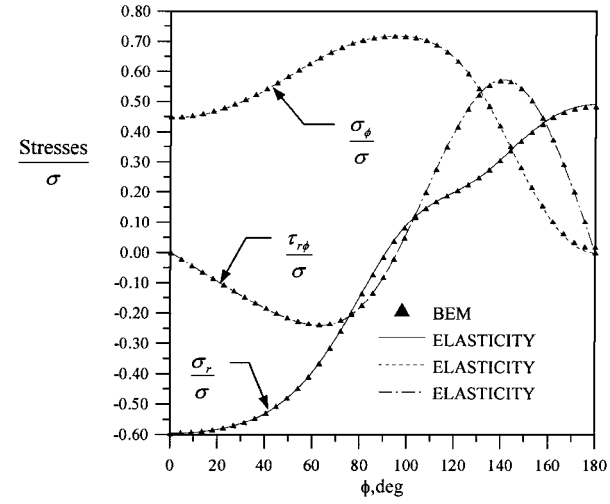

Fig. 13 Stress distribution along $r = 2R$ in the end eyebar plate: $b = 4R$ and $\bar{N} = 16$.

V. Boundary Element–Elasticity Solution of Pin-Loaded Plates

To illustrate the coupled boundary element–elasticity procedure, we present the analysis of three pin-loaded plates having potentially practical geometries. They are eyebars as shown in Fig. 7; rectangular plates with a circular edge, such as plate 1 as shown in Fig. 14; and full rectangular plates, such as plate 2 as shown in Fig. 15. In all examples, we assume $E = 57.85$ GPa, $\nu = 0.31$, $e = \mu = 0$, and all plates are under a uniform far-field stress σ. A total of 50 boundary elements for the models are used.

Eyebars

The radius of curvature $R_c = b$ for the transition curve (as shown in Fig. 7b) is used, where b is the radius of the outer surface of the pin-loaded annulus. Therefore, the angle θ determined from Eq. (27) becomes

$$\theta = \sin^{-1}[(b + d)/2b] \tag{32}$$

The geometrical dimensions of $L/R = 16$ and $H = 1$ mm are considered. The boundary tractions of the pin-loaded annulus determined by the boundary element solutions for eyebars with $b/R = 3$, 4, and 5 corresponding to $\theta = 56.54$, 48.59, and 44.43 deg, respectively, are obtained first. They are closely represented by Eqs. (28–31), as shown in Figs. 16–18, by taking $m_1 = m_3 = m_4 = 6$ for p_{ir}, p_{or}, and p_{ot}. The contact angles α rounded to the nearest degree are 92, 91, and 90 deg, respectively; the constants involved in Eqs. (28–31) for this case are shown in Table 2.

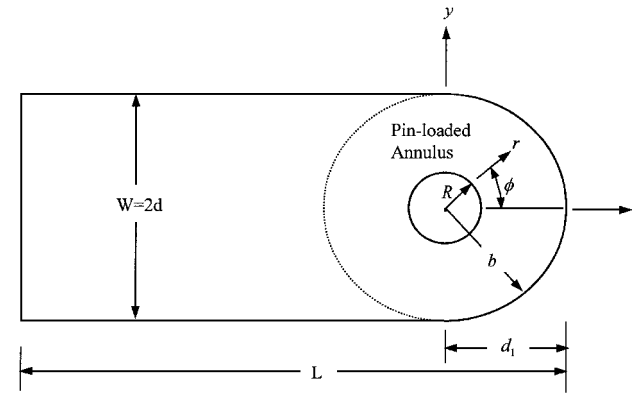

a) Rectangular plates with a circular edge

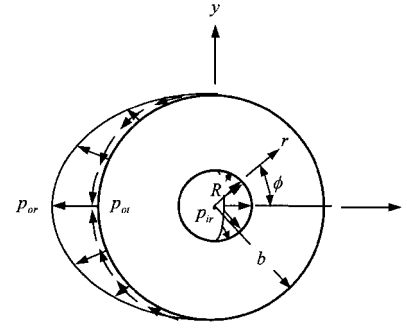

b) Stress distributions along the boundary

Fig. 14 Geometry, coordinate systems, and boundary tractions of pin-loaded rectangular plates with a circular edge.

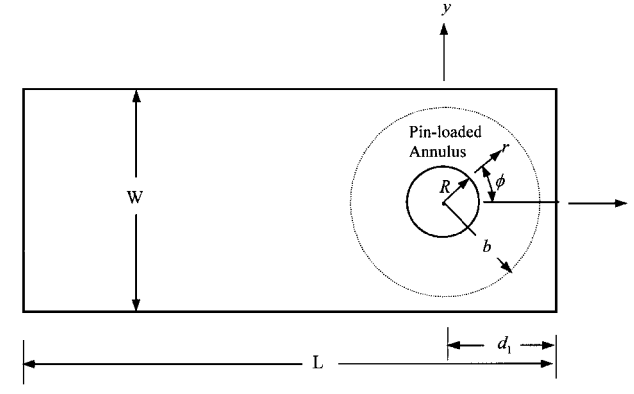

a) Geometry and coordinates

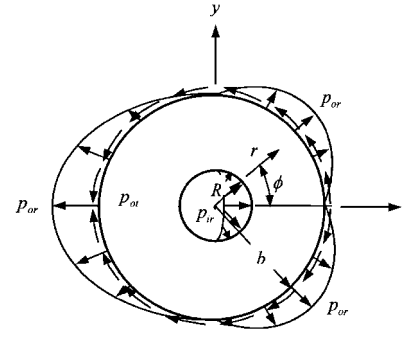

b) Boundary tractions of pin-loaded annulus

Fig. 15 Geometry, coordinate systems, and boundary tractions of pin-loaded rectangular plates.

Plate 1

The geometric shape with $b/R = 4$ for plate 1 is shown in Fig. 14. The dimensions are $L/R = 16$, $d_1/R = 5$, and $H = 1$ mm. The boundary tractions of the pin-loaded annulus along $r = R$ and b by the direct boundary element method using $m_1 = m_3 = m_4 = 6$ are shown in Figs. 18–20. The contact angle α rounded to the nearest degree is 87 deg, and the constants involved in Eqs. (28–31) are listed in Table 3.

Table 2 Constants A_m, B_m, and B_m^* for pin-loaded eyebars: $m_1 = m_3 = m_4 = 6$

	$b/R = 3$ ($\alpha = 92$ deg)			$b/R = 4$ ($\alpha = 91$ deg)			$b/R = 5$ ($\alpha = 90$ deg)		
m	$q_{ir}(A_m)$	$q_{or}(B_m)$	$q_{ot}(B_m^*)$	$q_{ir}(A_m)$	$q_{or}(B_m)$	$q_{ot}(B_m^*)$	$q_{ir}(A_m)$	$q_{or}(B_m)$	$q_{ot}(B_m^*)$
0	107.462	−13,391.014	——	138.243	−2,251.605	——	139.369	46,501.230	——
1	−195.260	−23,444.675	997.757	−250.498	−3,741.960	−1,403.469	−252.169	80,998.541	−4,208.346
2	137.772	−15,607.166	1,310.356	177.469	−2,089.906	−1,901.655	177.933	53,113.101	−5,528.350
3	−75.556	−7,705.987	947.260	−98.146	−701.415	−14,48.947	−97.869	25,579.681	−4,002.185
4	31.058	−2,677.446	421.827	40.656	−81.781	−698.063	40.173	8,592.216	−1,795.073
5	−8.670	−587.033	108.949	−11.427	28.067	−200.598	−11.138	1,807.421	−471.156
6	1.261	61.263	12.516	1.672	8.802	−26.464	1.596	179.883	−55.790

Table 3 Constants A_m, B_m, and B_m^* for plates 1 and 2: $m_1 = m_3 = m_4 = 6$

	Plate 1 ($\alpha = 87$ deg)			Plate 2 ($\alpha = 86$ deg)		
m	$q_{ir}(A_m)$	$q_{or}(B_m)$	$q_{ot}(B_m^*)$	$q_{ir}(A_m)$	$q_{or}(B_m)$	$q_{ot}(B_m^*)$
0	398.300	−9.708	——	358.844	0.274	——
1	716.413	−18.399	0.276	−645.665	−0.412	0.071
2	502.843	−12.805	−0.186	452.200	0.245	−0.365
3	−273.698	−7.539	0.126	−245.369	−0.088	0.179
4	110.492	−3.210	−0.129	98.723	−0.033	0.114
5	−29.920	−0.877	−0.146	−26.597	0.017	0.085
6	4.158	−0.112	−0.047	3.676	0.0005	0.053

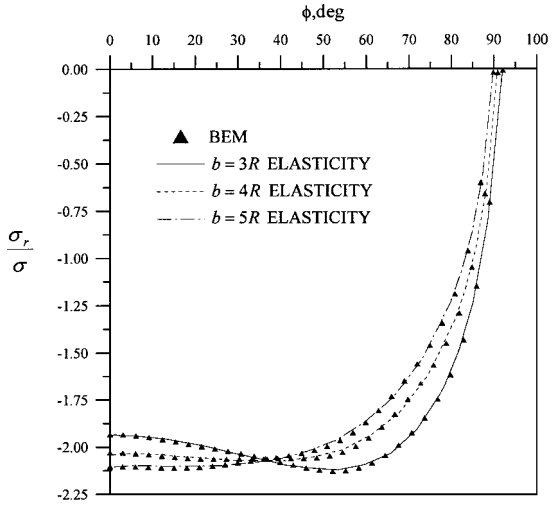

Fig. 16 Radial stress along the hole of eyebars: $m_1 = 6$.

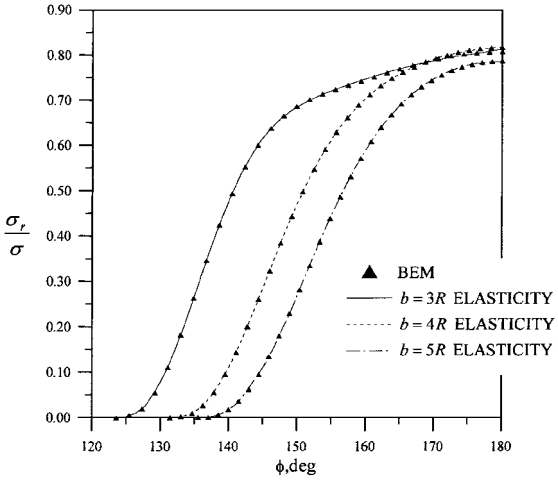

Fig. 17 Radial stress on the outer surface of pin-loaded annulus of eyebars: $m_3 = 6$.

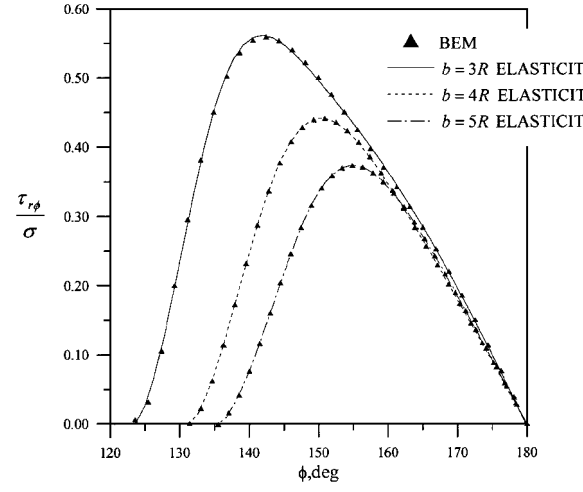

Fig. 18 Shear stress on the outer surface of pin-loaded annulus of eyebars: $m_4 = 6$.

Plate 2

A full rectangular plate with $b/R = 4$ is shown in Fig. 15. The geometrical dimensions are $L/R = 17$, $d_1/R = 5$, and $H = 1$ mm. The boundary tractions along $r = R$ and b found by the direct boundary element method using $m_1 = m_3 = m_4 = 6$ are shown in Figs. 19–21. The contact angle α rounded to the nearest degree is 86 deg, and the constants involved in Eqs. (28–31) are shown in Table 3.

Using the generated constants given in Table 2 or Table 3 for whichever case is under consideration, one can routinely calculate the Fourier coefficients given in Eqs. (A1–A14) in the Appendix for determining stresses and displacements at any point of interest in the pin-loaded annulus according to Eqs. (13–15), (17), and (18). Hence, the data presented in Tables 2 and 3 may be used for future reference or direct practical applications.

Example

For illustrative purposes, we consider the class of eyebars with $b/R = 3$, 4, and 5 and $e = \mu = 0$. The angles θ are 56.44, 48.59, and 44.43 deg; the contact angles α rounded to the nearest degree are 92, 91, and 90 deg, respectively. The constants given in Table 2 are used. The coupled boundary element–elasticity solutions are presented in Figs. 16–18 and 22. Figures 16–18 show close representations of boundary element data for the pin-loaded annulus using

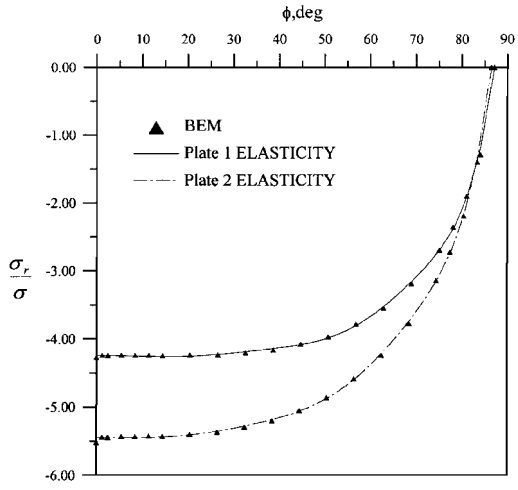

Fig. 19 Radial stress along the hole edge of plates 1 and 2: $m_1 = 6$.

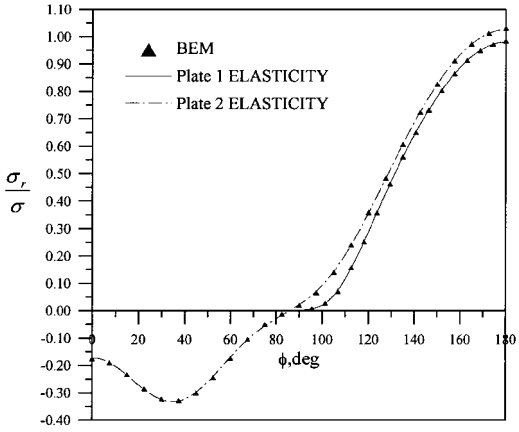

Fig. 20 Radial stress on the outer surface of pin-loaded annulus of plates 1 and 2: $m_3 = 6$.

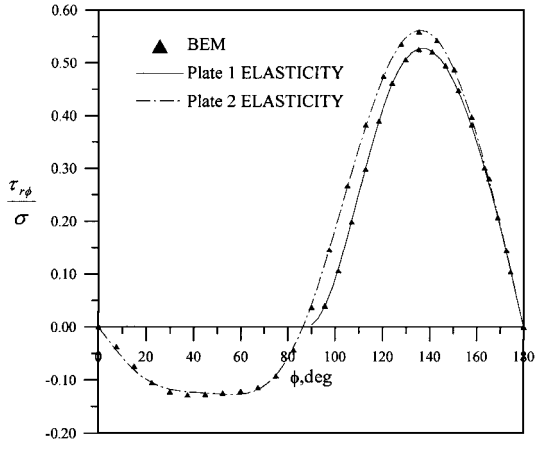

Fig. 21 Shear stress on the outer surface of pin-loaded annulus of plates 1 and 2: $m_4 = 6$.

Eqs. (28–31). Because the failure of isotropic eyebars would most likely to occur on the hole edge, the circumferential stresses σ_ϕ are computed there to provide the complete state of stress at points of the hole edge for potential examination against failure. Results on σ_ϕ computed using the elasticity solutions are as shown in Fig. 22. We have found that the use of the boundary element–elasticity solution scheme is efficient and more convenient than completely using the boundary element procedure.

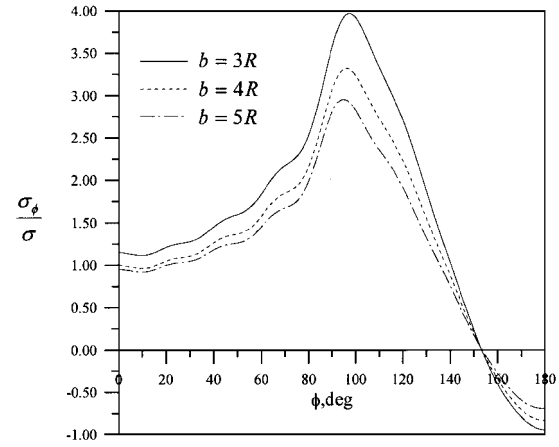

Fig. 22 Circumferential stress along hole edge of eyebars.

VII. Conclusions

A direct boundary element method was established and used successfully by Lin and Lin[23] in the study of stresses around pin-loaded holes of composite laminates. The method has been extended to include the determination of stresses and displacements at any point in the plate. The computational algorithm has also been refined and improved somewhat to enhance the efficiency. The method, procedure, and computer program have been verified by elasticity solutions numerically, using a variety of cases for plates with and without pins. A coupled boundary element–elasticity solution method is presented. The analysis procedure of the method, requiring minimal computational effort, is effective and efficient. The computational scheme, which is simple to use and provides accurate results, should be convenient for direct practical applications.

Appendix: Solutions for a_n, b_n, a'_n, and b'_n

The Fourier coefficients for annulus plates of a_n, b_n, a'_n, and b'_n are obtained as follows:

$$a_0 = \frac{R^2 b^2}{\pi(b^2 - R^2)}\left[A_0\alpha - B_0\theta + \sum_{m=1}^{m_1}\frac{A_m}{m}\sin m\alpha + \sum_{m=1}^{m_3}\frac{B_m}{m}\sin m(\pi - \theta)\right] \tag{A1}$$

$$b_0 = \frac{1}{2\pi(b^2 - R^2)}\left[-A_0 R^2\alpha + B_0 b^2\theta - \sum_{m=1}^{m_1}\frac{R^2 A_m}{m}\sin m\alpha + \sum_{m=1}^{m_3}\frac{b^2 B_m}{m}\sin m(\pi - \theta)\right] \tag{A2}$$

$$a_1 = \frac{R}{\pi}\left[A_1\alpha - A_0\sin\alpha + \sum_{m=0}^{m_1}\frac{A_m}{m+1}\sin(m+1)\alpha + \sum_{m=2}^{m_1}\frac{A_m}{m-1}\sin(m-1)\alpha\right] - \frac{R}{\pi}\left[A_1^*\alpha - \sum_{m=1}^{m_2}\frac{A_m^*}{m+1}\times\sin(m+1)\alpha + \sum_{m=2}^{m_2}\frac{A_m^*}{m-1}\sin(m-1)\alpha\right] \tag{A3}$$

$$b_1 = \frac{1}{2(b^4 - R^4)}\left[-(b^2 - R^2)b'_1 + b^3 S_4 - R^3 S_2\right] \tag{A4}$$

$$a'_1 = \frac{R^4 b^4}{2(b^4 - R^4)}\left[\frac{(b^2 - R^2)b'_1}{b^2 R^2} + \frac{S_4}{b} - \frac{S_2}{R}\right] \tag{A5}$$

$$b'_1 = \frac{-a_1(1 - \nu)}{4} \tag{A6}$$

where

$$S_2 = \frac{1}{\pi}\left[A_1^*\alpha - \sum_{m=1}^{m_2} \frac{A_m^*}{m+1}\sin(m+1)\alpha + \sum_{m=2}^{m_2} \frac{A_m^*}{m-1}\sin(m-1)\alpha \right] \tag{A7}$$

$$S_4 = B_1^* + \frac{1}{\pi}\left[-B_1^*(\pi-\theta) + \sum_{m=1}^{m_4} \frac{B_m^*}{m+1}\sin(m+1)(\pi-\theta) - \sum_{m=2}^{m_4} \frac{B_m^*}{m-1}\sin(m-1)(\pi-\theta) \right] \tag{A8}$$

and the coefficients of a_n, b_n, a'_n, and b'_n for $n = 2, 3, \ldots, \bar{N}$ are determined from the following equations in matrix form:

$$\begin{Bmatrix} a_n \\ b_n \\ a'_n \\ b'_n \end{Bmatrix} = \left[\bar{C}\right]^{-1} \begin{Bmatrix} S_{n1} \\ S_{n2} \\ S_{n3} \\ S_{n4} \end{Bmatrix} \tag{A9}$$

with

$$\left[\bar{C}\right] = \begin{bmatrix} -n(n-1)R^{n-2} & -(n-2)(n+1)R^n & -n(n+1)R^{-(n+2)} & -(n+2)(n-1)R^{-n} \\ n(n-1)R^{n-2} & n(n+1)R^n & -n(n+1)R^{-(n+2)} & -n(n-1)R^{-n} \\ -n(n-1)b^{n-2} & -(n-2)(n+1)b^n & -n(n+1)b^{-(n+2)} & -(n+2)(n-1)b^{-n} \\ n(n-1)b^{n-2} & n(n+1)b^n & -n(n+1)b^{-(n+2)} & -n(n-1)b^{-n} \end{bmatrix} \tag{A10}$$

$$S_{n1} = \frac{2}{\pi}\int_0^{\alpha} p_{ir}\cos n\phi \, d\phi = \begin{cases} \frac{2}{\pi}\left[\frac{A_0}{n}\sin n\alpha + \sum_{m=1}^{m_1} \frac{A_m}{m^2-n^2}(m\cos n\alpha \sin m\alpha - n\cos m\alpha \sin n\alpha) \right] & \text{for} \quad m \neq n \\ \frac{2}{\pi}\left[\frac{A_0}{n}\sin n\alpha + \left(\frac{\alpha}{2} + \frac{1}{4n}\sin 2n\alpha\right) \right] & \text{for} \quad m = n \end{cases} \tag{A11}$$

$$S_{n2} = \frac{2}{\pi}\int_0^{\alpha} p_{it}\sin n\phi \, d\phi = \begin{cases} \frac{2}{\pi}\left[\sum_{m=1}^{m_2} \frac{A_m^*}{m^2-n^2}(n\cos n\alpha \sin m\alpha - m\cos m\alpha \sin n\alpha) \right] & \text{for} \quad m \neq n \\ \frac{2}{\pi}\left[\frac{\alpha}{2} - \frac{1}{4}\sin 2n\alpha \right] & \text{for} \quad m = n \end{cases} \tag{A12}$$

$$S_{n3} = \frac{2}{\pi}\int_{\pi-\theta}^{\pi} p_{or}\cos n\phi \, d\phi = \begin{cases} \frac{2}{\pi}\left[\frac{-B_0}{n}\sin n(\pi-\theta) + \sum_{m=1}^{m_3} \frac{B_m}{m^2-n^2}(-m\cos n(\pi-\theta) \times \sin m(\pi-\theta) + n\cos m(\pi-\theta)\sin n(\pi-\theta)) \right] & \text{for} \quad m \neq n \\ \frac{2}{\pi}\left[\frac{-B_0}{n}\sin n(\pi-\theta) + \left(\frac{\theta}{2} - \frac{1}{4n}\sin 2n(\pi-\theta)\right) \right] & \text{for} \quad m = n \end{cases} \tag{A13}$$

$$S_{n4} = \frac{2}{\pi}\int_{\pi-\theta}^{\pi} p_{ot}\sin n\phi \, d\phi = \begin{cases} \frac{2}{\pi}\left[\sum_{m=1}^{m_4} \frac{B_m^*}{m^2-n^2}(-n\cos n(\pi-\theta)\sin m(\pi-\theta) + m\cos m(\pi-\theta)\sin n(\pi-\theta)) \right] & \text{for} \quad m \neq n \\ \frac{2}{\pi}\left[\frac{\theta}{2} + \frac{1}{4n}\sin 2n(\pi-\theta) \right] & \text{for} \quad m = n \end{cases} \tag{A14}$$

Note that the quantities S_{n1}, S_{n2}, S_{n3}, and S_{n4} in Eqs. (A11–A14) corresponding to Eqs. (28–31) have been explicitly obtained. The integrals involved in various quantities can be directly evaluated by MATHEMATICA once p_{ir}, p_{it}, p_{or}, and p_{ot} are specified.

Acknowledgment

The study was supported by the National Science Council of Taiwan, Republic of China, under Grant NSC 88-2212-E-005-001.

References

[1] Jong, T. D., "Stresses Around Pin-Loaded Holes in Elastically Orthotropic or Isotropic Plates," *Journal of Composite Materials*, Vol. 11, 1977, pp. 313–331.

[2] Zhang, K. D., and Ueng, C. E. S., "Stresses Around a Pin-Loaded Hole in Orthotropic Plates," *Journal of Composite Materials*, Vol. 18, 1984, pp. 432–446.

[3] Eshwar, V. A., "Analysis of Clearance Fit Pin Joints," *International Journal of Mechanical Science*, Vol. 20, 1978, pp. 485–491.

[4] Ghosh, B. D., and Rao, A. K., "Load Transfer from a Smooth Elastic Pin to a Large Sheet," *AIAA Journal*, Vol. 18, No. 5, 1981, pp. 619–625.

[5] Mangalgiri, P. D., Ramamurthy, T. S., Dattaguru, B., and Rao, A. K., "Elastic Analysis of Pin Joints in Plates Under Some Combined Pin and Plate Loads," *International Journal of Mechanical Science*, Vol. 28, No. 8, 1987, pp. 577–585.

[6] Chang, F. K., Scott, R. A., and Springer, G. S., "Strength of Mechanically Fastened Composite Joints," *Journal of Composite Materials*, Vol. 16, 1983, pp. 470–494.

[7] Chang, F. K., and Scott, R. A., "Failure of Composite Laminates Containing Pin Loaded Holes-Method of Solution," *Journal of Composite Materials*, Vol. 18, 1984, pp. 255–278.

[8] Chang, F. K., and Scott, R. A., "Failure Strength of Nonlinearly Elastic Composite Laminates Containing a Pin Loaded Hole," *Journal of Composite Materials*, Vol. 18, 1984, pp. 464–477.

[9] Chang, F. K., "The Effect of Pin Load Distribution on the Strength of Pin Loaded Holes in Laminated Composites," *Journal of Composite Materials*, Vol. 20, 1986, pp. 401–408.

[10] Tsujimoto, Y., and Wilson, D., "Elasto-Plastic Failure Analysis of Composite Bolted Joints," *Journal of Composite Materials*, Vol. 20, 1986, pp. 236–252.

[11] Wong, S., and Matthews, F. L., "A Finite Element Analysis of Single and Two-Hole Bolted Joints in Fibre Reinforced Elastic," *Journal of Composite Materials*, Vol. 15, 1981, pp. 481–491.

[12] Blackie, A. P., and Chutima, S., "Stress Distributions in Multi-Fastened Composite Plates," *Composite Structures*, Vol. 34, 1996, pp. 427–436.

[13] Waszczak, J. P., and Cruse, T. A., "Failure Mode and Strength Predictions of Anisotropic Bolt Bearing Specimens," *Journal of Composite Materials*, Vol. 5, 1971, pp. 421–425.

[14] Mahajerin, E., and Sikarskin, D. L., "Boundary Element Study of a Loaded Hole in an Orthotropic Plate," *Journal of Composite Materials*, Vol. 20, 1986, pp. 375–389.

[15] Lin, C. C., and Lin, C. H., "Stress and Strength Analysis of Bolted Composite Joints Using Direct Boundary Element Method," *Journal of Composite Structures*, Vol. 25, 1993, pp. 209–215.

[16]Hyer, M. W., and Klang, E. C., "Contact Stresses in Pin-Loaded Orthotropic Plates," *International Journal of Solids and Structure*, Vol. 21, No. 9, 1985, pp. 957–975.

[17]Hyer, M. W., Klang, D. C., and Cooper, D. E., "The Effects of Pin Elasticity, Clearance, and Friction on the Stresses in a Pin-Loaded Orthotropic Plate," *Journal of Composite Materials*, Vol. 21, 1987, pp. 190–206.

[18]Yogeswaren, E. K., and Reddy, J. N., "A Study of Contact Stresses in Pin-Loaded Orthotropic Plates," *Computers and Structures*, Vol. 30, No. 5, 1988, pp. 1067–1077.

[19]Rahman, M. U., and Rowlands, R. E., "Finite Element Analysis of Multiple Bolted Joints in Orthotropic Plates," *Computers and Structures*, Vol. 46, No. 5, 1993, pp. 859–867.

[20]Agarwal, B. L., "Static Strength Prediction of Bolted Joint in Composite Material," *AIAA Journal*, Vol. 18, No. 11, 1980, pp. 1371–1375.

[21]Rahman, M. U., "An Iterative Procedure for Finite-Element Stress Analysis of Frictional Contact Problems," *Computers and Structures*, Vol. 18, 1984, pp. 947–954.

[22]Naik, R. A., and Crews, J. H., Jr., "Stress Analysis Method for a Clearance-Fit Bolt," *AIAA Journal*, Vol. 24, No. 8, 1986, pp. 1348–1353.

[23]Lin, C. C., and Lin, C. H., "Stresses Around Pin-Loaded Hole in Composite Laminates Using Direct Boundary Element Method," *International Journal of Solids and Structures*, Vol. 36, 1999, pp. 763–783.

[24]Quinn, W. J., and Matthews, F. L., "The Effect of Stacking Sequence on the Pin-Bearing Strength in Glass Fibre Reinforced Plastic," *Journal of Composite Materials*, Vol. 11, 1977, pp. 139–145.

[25]Pyner, G. R., and Matthews, F. L., "Comparison of Single and Multihole Bolted Joints in Glass Fibre Reinforced Plastic," *Journal of Composite Materials*, Vol. 13, 1979, pp. 232–239.

[26]Tsai, M. Y., and Morton, J., "Stress and Failure Analysis of Pin-Loaded Composite Plate: An Experimental Study," *Journal of Composite Materials*, Vol. 24, 1990, pp. 1101–1121.

[27]Cooper, C., and Turvey, G. J., "Effects of Joint Geometry and Bolt Torque on the Structural Performance of Single Bolt Tension Joints in Pultruded GRP Sheet Material," *Composite Structures*, Vol. 32, 1995, pp. 217–226.

[28]Lin, C. H., "Analysis of Pin-Loaded Plates by a Boundary Element Method," Ph.D. Dissertation, National Chung-Hsing Univ., Taichung, Taiwan, ROC, 1998, Chaps. 5 and 6.

[29]Timoshenko, S. P., and Goodier, J. N., *Theory of Elasticity*, McGraw–Hill, New York, 1970.

[30]Lekhnitskii, S. G., Tsai, S. W., and Cheron, T., *Anisotropic Plates*, Gordon and Breach, New York, 1968.

S. Saigal
Associate Editor